Macromolecular Rapid Communications
www.mrc-journal.de

Croconaine-Based Polymer Particles as Contrast Agents for Photoacoustic Imaging

*Felicitas Jansen, Markus Lamla, Diana Mauthe, Stephan Fischer, Holger Barth, and Alexander J. C. Kuehne**

In the development and optimization of imaging methods, photoacoustic imaging (PAI) has become a powerful tool for preclinical biomedical diagnosis and detection of cancer. PAI probes can improve contrast and help identify pathogenic tissue. Such contrast agents must meet several requirements: they need to be biocompatible, and absorb strongly in the near-infrared (NIR) range, while relaxing the photoexcited state thermally and not radiatively. In this work, polymer nanoparticles are produced with croconaine as a monomer unit. Small molecular croconaine dyes are known to act as efficient pigments, which do not show photoluminescence. Here, for the first time croconaine copolymer nanoparticles are produced from croconic acid and a range of aromatic diamines. Following a dispersion polymerization protocol, this approach yields monodisperse particles of adjustable size. All synthesized polymers exhibit broad absorption within the NIR spectrum and therefore represent suitable candidates as contrast agents for PAI. The optical properties of these polymer particles are discussed with respect to the relation between particle size and outstanding photoacoustic performance. Biocompatibility of the polymer particles is demonstrated in cell viability experiments.

Photoacoustic imaging (PAI) is a powerful non-invasive bioimaging modality with superior penetration depth compared to conventional light-based imaging techniques.[1–3] While PAI is currently limited to preclinical research, it has high potential to become a standard imaging technique for screening, diagnosis, and therapeutic monitoring of cancer.[4,5] For light-based imaging techniques, the strong scattering, and absorption in biological tissue is a challenging problem, as light has to pass tissue twice for excitation and detection. PAI circumvents this drawback by limiting the light path to only excitation, while detection is performed using ultrasound, produced by endogenous or exogenous contrast agents.[6] Contrast is obtained by the photoacoustic effect, where ultrasound pressure waves are generated by an alternating thermoelastic expansion and contraction of the absorbing imaging probes. These pressure waves are induced by pulsed laser irradiation. When using pulsed, non-ionizing near-infrared (NIR) excitation, attenuation of light by tissue and skin as well as background autofluorescence are minimal—this effect is known as the NIR tissue transparency window.[7–10] Within this spectral range it is possible to achieve deep tissue penetration of up to 7 cm, while maintaining high spatial resolution.[11,12] PAI enables imaging of oxygenated and deoxygenated hemoglobin molecules due to the different absorption profiles of these endogenous contrast agents.[13] However, imaging of pathological tissue usually requires some strategy of targeting, using artificial contrast agents because endogenous imaging probes provide insufficient signal-to-noise ratio.[14] Therefore, it is crucial to develop efficient exogenous contrast agents to allow precise and spatially localized staining and well resolved imaging.[15] Current developments make use of the full range from small molecule tracers, to polymers and particles.[16–19] In the area of particle-based PAI,[20] gold nanoparticles have gathered attraction because of their variable plasmon resonance, which for high aspect ratio nanostructures can be shifted into the NIR range.[21] However, well-performing gold nanorods exhibit relatively high cytotoxicity, strongly limiting clinical application of these particles.[14] By contrast, organic dyes and polymers have high absorption efficiencies and low cytotoxicity and therefore represent more suitable agents as NIR absorbers for PAI.[22,23] Within this class of compounds, especially oxocarbon dyes such as squaraine and croconaine dyes are promising candidates for PAI, because of their tendency to relax the photoexcited state thermally. However, the absorption maximum of these dyes is usually located in the visible and maybe the deep red spectrum—just outside the tissue transparency window.[24] This lack of absorption in the NIR spectrum

F. Jansen, Prof. A. J. C. Kuehne
DWI—Leibniz Institute for Interactive Materials
Forckenbeckstraße 50, Aachen 52074, Germany
E-mail: alexander.kuehne@uni-ulm.de
Dr. M. Lamla, D. Mauthe, Prof. A. J. C. Kuehne
Institute of Macromolecular and Organic Chemistry
Ulm University
Albert-Einstein-Allee 11, Ulm 89081, Germany
Dr. S. Fischer, Prof. H. Barth
Institute of Pharmacology and Toxicology
Ulm University Medical Center
Albert-Einstein-Allee 11, Ulm 89081, Germany
The ORCID identification number(s) for the author(s) of this article can be found under https://doi.org/10.1002/marc.202000418.

DOI: 10.1002/marc.202000418

prevents photoacoustic applications, as strong absorption in the NIR region is a crucial requirement for good PAI. Extension of the π-conjugated system, for example, by fusing chromophores into polymers, induces a bathocromical shift and broadening of the absorption peak.[25] Polymers based on conjugated donor and croconic acid acceptor units could therefore enable strong absorption in the NIR spectrum and become promising materials for PAI, due to the intrinsic thermal relaxation upon photoexcitation. Only few croconaine polymers have previously been synthesized successfully.[25,26] Due to their low solubility in water as well as organic solvents, characterization and handling is difficult and has prevented applications of these interesting materials in optoelectronics or biomedical imaging to date. Shaping polymers into particles could improve handling of these agents, simplify their characterization, and allow their use as contrast agents in PAI. However, suitable synthetic protocols toward croconaine polymer particles are absent to date.

In this work, we present the synthesis of monodisperse polymer nanoparticles using croconic acid as the basic acceptor building block and various diamines as donor co-monomer. Due to the produced electronically extended chromophore system, all synthesized polymers exhibit broad absorption within the "tissue transparency window." These outstanding optical properties together with the thermal relaxation of the photoexcited state, render these particles ideal candidates for PAI.

Croconaine dyes are synthesized by condensing strongly electron accepting croconic acid with two equivalents of aromatic or heterocyclic donor moieties.[24,27] Although the exact reaction mechanism has not been completely unraveled, all syntheses produce water as a by-product and its removal is utilized as the driving force of the reaction. Formally, a hydrogen atom of the donor molecule and a hydroxy group of the croconic acid are eliminated producing the coupled product. Interestingly, this condensation works also for aromatic amines, where C—N bonds are formed after elimination of water. The primary amine is converted to a secondary amine by reacting with croconic acid, enabling hydrogen bonding of the amine hydrogen and the croconic carbonyl groups, constraining the aromatic system into a planar delocalized conformation. The simplest form of this dye **C1** is produced by condensation of croconic acid with aniline (**Figure 1**a, Figures S1 and S2a, Supporting Information).[28]

To produce a polymer by this condensation reaction, we employ 1,4-phenylenediamine as a bifunctional monomer, for which polymerization has been shown before.[26] The obtained polymer is hardly soluble in organic solvents due to its rigid backbone, tendency to aggregate due to strong π-interactions, and lack of solubilizing peripheral units.[25] While this insolubility is a drawback for characterization, it represents an integral part of the particle formation mechanism of the dispersion polymerization technique. Dispersion polymerization

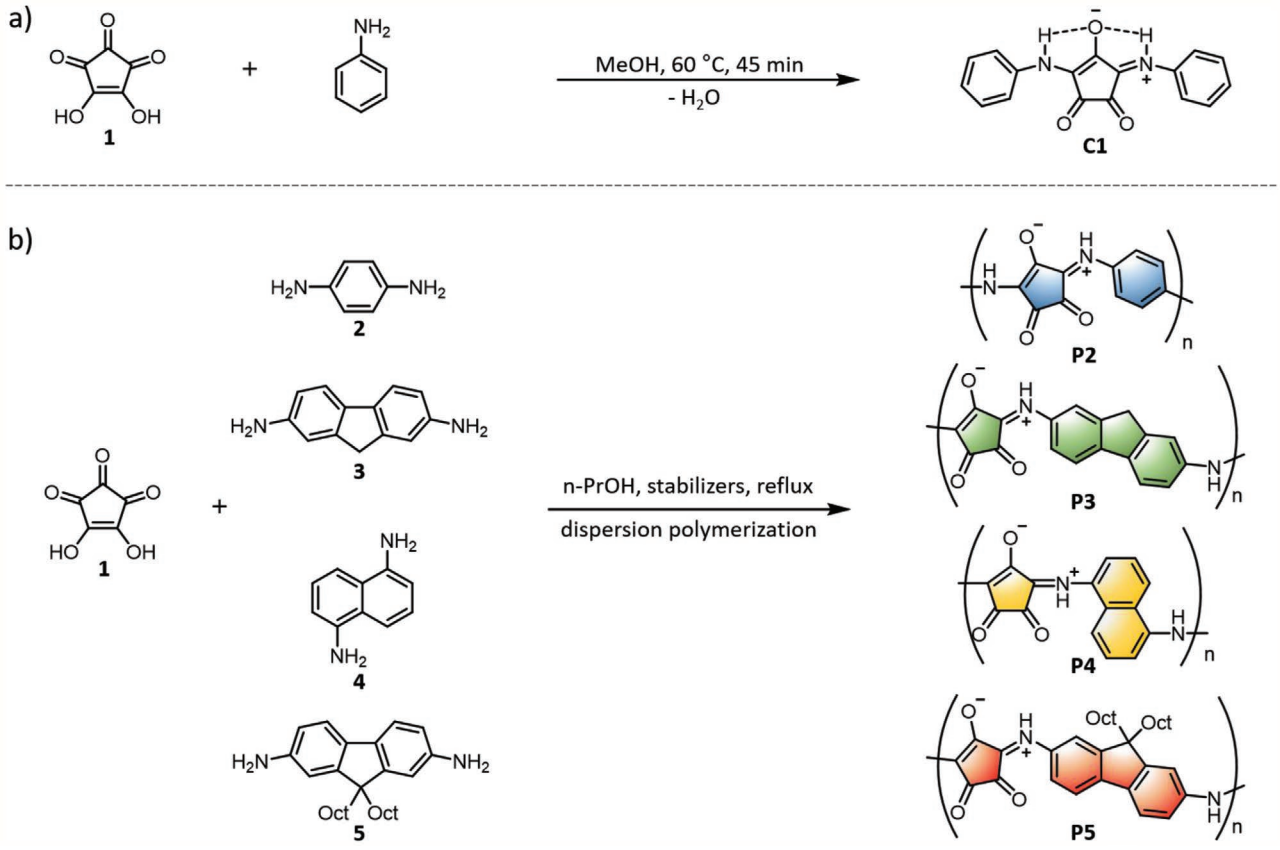

Figure 1. a) Formation of a croconaine dye (**C1**) by condensation of croconic acid (**1**) and two equivalents of aniline in methanol according to the synthetic procedure described in the literature.[28] b) Synthesis of polymer nanoparticles. Dispersion polycondensation with croconic acid (**1**) and diamine-based monomers (**2**–**5**) to produce the respective polymers (**P2**–**P5**).

implies that initially all low molecular reagents are soluble in the applied solvent. During polymerization, the polymer chains grow and become insoluble. At this point the polymer chains phase separate and form nuclei, onto which other polymer chains can condensate to grow the final particles.[29] The particles are stabilized against aggregation by admixed dispersants. Although formally there is no extended conjugated system along the entire polymer, we assume that the positive charge is delocalized over the nitrogen atoms and therefore croconaine-based polymers are considered to be quasi-conjugated.

To produce our croconaine nanoparticles, we apply croconic acid (**1**) together with stoichiometric amounts of one of four different diamines (**2**–**5**) in 1-propanol and with poly(1-vinylpyrrolidone-*co*-vinyl acetate) (PVPVA) and Triton X-45 as dispersants (Figure 1b). We apply as much as 90 g L^{-1} of PVPVA to obtain more amorphous particle morphologies, as we have established previously.[30] Refluxing the reaction mixtures leads to a color shift from yellow to black indicating the formation of a delocalized π-conjugated system. After purification by centrifugation, we analyze the obtained polymer particles by scanning electron microscopy (SEM). While we obtain platelet like and presumably crystalline precipitates for monomers **2** and **3**, almost spherical, and therefore more amorphous particles are obtained for monomers **4** and **5** (**Figure 2**a–d). Breaking of the linear polymer structure and introduction of sterically demanding alkyl chains represent means to reduce crystallinity and obtain monodisperse, amorphous polymer particles in the submicrometer range, as shown in Figure 2d. The synthesized particles are well dispersible in many organic solvents as well as in water. The particles are insoluble in almost all solvents, which is why we apply mass spectrometry (MS) (MALDI-FTICR) to confirm that indeed polymer chains make up the particles, instead of low-molecular-weight oligomers (Figure S2b, Supporting Information). We can detect molecules with a degree of polymerization of 18 repeat units; however, we assume we might form even higher molar masses, which we cannot detect by MS. We have previously observed that small quantities of the stabilizer PVPVA become incorporated into the particles.[29] Here, analysis is difficult as the croconaine-based polymer particles are hardly soluble. We could estimate by elemental analysis that up to 8 wt% of the particle consists of PVPVA (see Experimental Section).

To investigate the optical and photoacoustic performance, which we need for our desired bioimaging applications, we perform UV/vis spectroscopy and PAI. While we expect scattering of the particles toward the blue end of the vis-spectrum, we clearly see the absorption maxima above 700 nm for all polymer particles (**P2**–**P5**) with broad absorption across the whole NIR range. In contrast to the small molecular croconaine dye (**C1**), the absorption bands of our polymer particles are strongly bathochromically shifted and broadened due to the extended

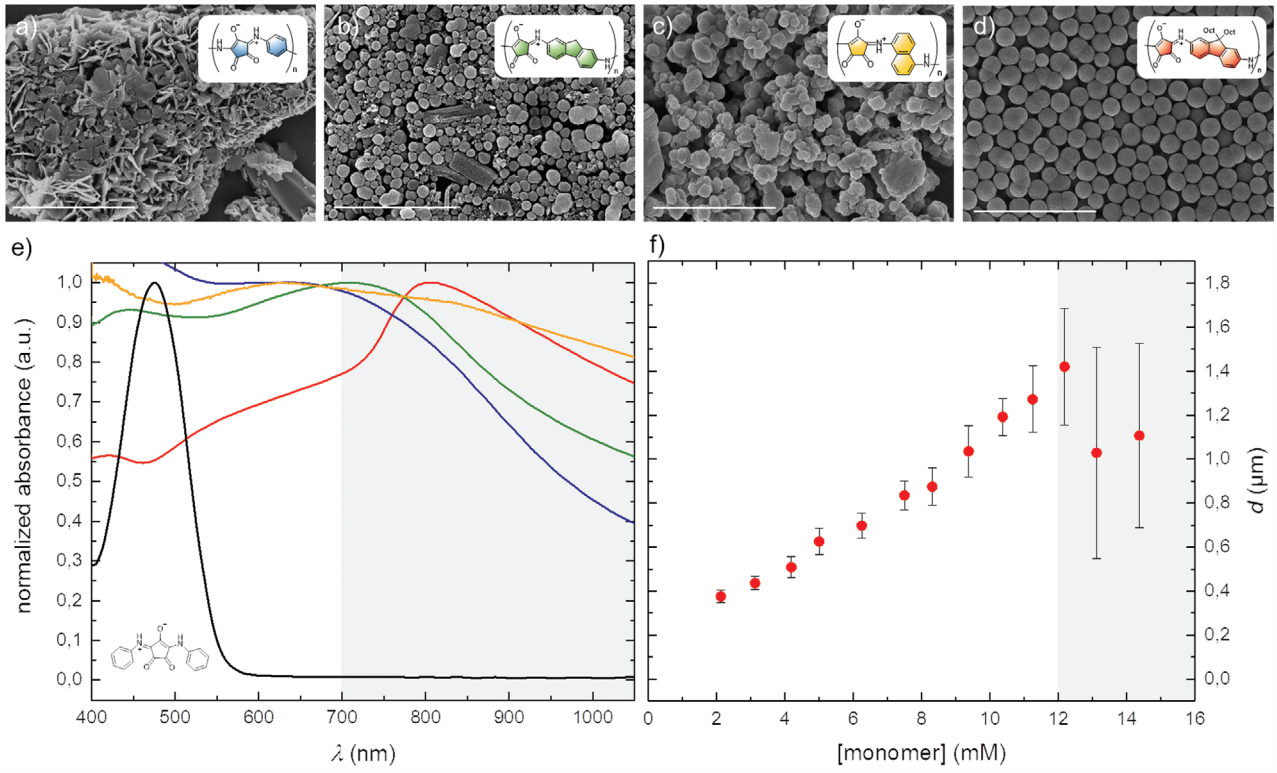

Figure 2. a–d) SEM images of croconaine-based polymers. The insets show the structures of the respective polymers (**P2**–**P5**). All scale bars represent 5 µm. e) UV/vis spectrum of all synthesized diamine-based polymers. The blue curve represents **P2**, the green curve represents **P3**, the grey curve represents **P3**, and the red curve represents **P5**. All polymers show a broad absorption within the tissue transparency window (grey shaded area). The UV/vis measurements of the polymers are carried out in water. The black curve is the absorption spectrum of the croconaine dye **C1** based on aniline with a maximum at 475 nm. The spectrum is recorded in 1-propanol. f) Development of **P5** particle size with increasing amount of monomer. The error bars specify the particle dispersity. The grey-shaded area indicates a regime, where the obtained particles show high polydispersity.

chromophore system (Figure 2e). When we vary the initial monomer concentrations, while keeping all other parameters constant, we gain control of the size of the monodisperse particles and we can tune the diameter between 380 nm and 1.2 µm (Figure 2f). At lower monomer amounts, we observe no particle formation. When using more than 12 mM of monomer, secondary nucleation takes place leading to a broad particle size distribution. We monitor the absorption of the synthesized monodisperse particles and observe a shift to higher wavelengths with increasing particle size for the **P5** particles (Figure S3, Supporting Information). A possible explanation for this bathocromic shift is the formation of J-aggregates with increasing particle size.[31] However, XRD analysis of our **P5** particles does not provide evidence for this type of order. The particles appear amorphous (Figure S4, Supporting Information). Alternatively, the red shift can be explained by the size of the polymer chains. It is described in the literature that in polycondensation reactions for particle synthesis the critical molecular weight increases as the polymerization proceeds.[32] The reason for this increase might be found in the solubility product that increases because of the continued phase separation of polymers during dispersion polymerization. With progressing polymerization, longer and longer polymers can form in solution before reaching the solubility limit. Longer polymer chains imply that the chromophoric systems become even more extended, thus shifting the absorption of the particles to longer wavelengths.

Kinetic studies show that particle growth is almost complete after only 7 min, which is confirmed by SEM image analysis. Also the bathochromic shift of the absorption spectrum can be utilized to probe the kinetics. When relating the absorption maximum to the reaction time, a limited saturation function is obtained, representing the kinetic course for particle formation (Figure S5a,b, Supporting Information). Saturation is reached after less than 10 min, which provides further evidence for the rapid particle growth in the first minutes after starting the reaction.

For investigating the photoacoustic performance, we disperse defined amounts of particles in water and fill the dispersions into so called phantoms—which in our case is air-bubble free plastic tubing. We perform ultrasound (reflectance) imaging as well as PAI at four different wavelengths, between 750 and 920 nm within the tissue transparency window. We overlay the photoacoustic signal with the ultrasound reflection image, which we obtain from the same ultrasound transducer. We observe the highest photoacoustic activity for all polymers at 820 nm, but also at 850 nm, and 920 nm strong signal is obtained (**Figure 3**a). In contrast to the strong absorbance at

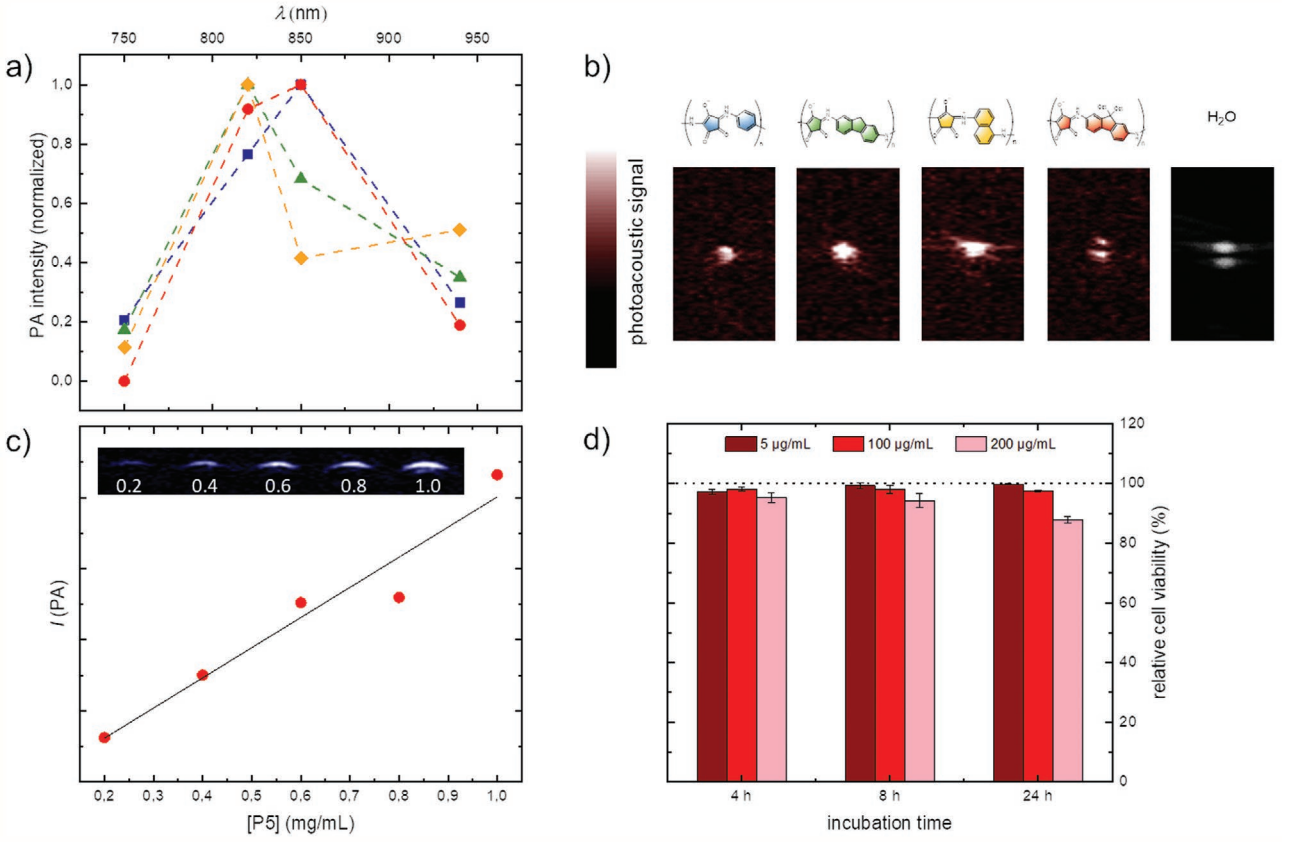

Figure 3. a) Normalized photoacoustic response as a function of wavelengths for **P2**–**P5**. b) Photoacoustic response of the different diamine-based polymers excited at a wavelength of $\lambda = 820$ nm. Pure water is used as reference. For water only the ultrasound signal is displayed, as no photoacoustic signal is produced. c) Concentration dependency of the photoacoustic signal of polymer **P5**. The inset shows the photoacoustic response of the corresponding polymer concentrations. d) Biocompatibility of the **P5** nanoparticles determined in a HeLa cytotoxicity assay. Three different particle concentrations are tested after incubation for 4, 8, and 24 h.

750 nm, the photoacoustic response is only of limited intensity. This unexpected inefficiency is most likely the result of competing absorption of water at this wavelength, which exhibits a local extinction maximum at 750 nm.[33] As expected, we detect no photoacoustic signal for pure water, which we employ as a control, here the image shows only ultrasound reflectance (Figure 3b). All particles **P2–P5** exhibit strong photoacoustic response to excitation at 820 nm. Due to the amorphous morphology of **P5** particles, thermal relaxation of the excited state might be slightly diminished compared to **P2–P4**. However, we continue with the **P5** particles, due to their much better colloidal stability and control over their size and shape during synthesis, making them suitable candidates for biomedical imaging applications. Therefore, we conduct more detailed photoacoustic measurements for the polymer particles **P5**. Excitation at of 820 nm shows that there is a linear relationship between the photoacoustic response and particle concentration, as shown in Figure 3c. Even at low concentrations of 0.2 mg mL^{-1}, we observe a photoacoustic signal, which highlights the high potential of the synthesized particles as contrast agents for biomedical imaging. To test whether the particles are stable in biological fluids and cell media, we perform dynamic light scattering (DLS) in deionized water and DMEM cell medium. This study shows that our particles do not aggregate in these fluids (Figure S6a, Supporting Information). **P5** particles with a size of 800 nm as determined by SEM exhibit a hydrodynamic radius of less than 1000 nm in water as well as in the cell medium. Therefore, we consider the particles to be well stable and dispersible in both water and DMEM cell media. As the environment of tumors is often acidic with pH 5.5–7,[34,35] we also perform colloidal stability tests using DLS at varying pH (Figure S6b, Supporting Information). **P5** particles of 400 nm in diameter do not aggregate between pH 3–14, proving their suitability as biomedical contrast agents.

To obtain information about the biocompatibility of the **P5** nanoparticles, we perform cell viability studies with HeLa cells. We observe relative cell viabilities of about unity for particle concentrations of 5 and 100 μg mL^{-1} and even at a particle concentration of 200 μg mL^{-1}, we still maintain high relative cell viability of more than 80% after 24 h, which should be sufficient considering the intended application as biomedical contrast agents (Figure 3d).

In conclusion, we have successfully synthesized croconaine-based polymer nanoparticles. These entities show great performance as NIR absorbers and photoacoustic contrast agents, while exhibiting good cell viability. With their diameters of several hundred nanometers to micrometers, such croconaine particles could find application in intestinal imaging applications. When decorated with biomedical recognition motifs these particles could be targeted toward malignant tumors.

Experimental Section

Chemicals: The following chemicals were purchased from Sigma-Aldrich/Merck: 2,7-diamino-fluorene with a purity of >97%, aniline, Triton X-45, PVPVA (average MW ≈ 50 000 Da), propidium iodide, fluorescein diacetate, methanol, and 1-propanol. Croconic acid with a purity of 98%, 2,7-diamino-9,9-di-n-octylfluorene with a purity of >98%, 1,4-phenylenediamine with a purity of >98% were purchased from TCI Chemicals. 1,5-diaminonaphthalene with a purity of 97% was obtained from Alfa Aesar. All chemicals and solvents were used without further purification.

Synthetic Procedure for Polymerization: PVPVA (720 mg) and Triton X-45 (800 mg) were dissolved in 1-propanol (3 mL). In a 25 mL round-bottom flask 2,7-diamino-9,9-di-n-octylfluorene (**5**) (21.0 mg, 0.05 mmol) and croconic acid (**1**) (7.1 mg, 0.05 mmol) were mixed with 1-propanol (5 mL). After addition of the stabilizers, the reaction flask was charged with a stirrer bar, sealed with a rubber septum, and degassed with argon for 10 min. Then, the yellow-colored mixture was transferred into a 120 °C oil bath and refluxed for 24 h under exclusion of oxygen. After 2 min, the color of the reaction mixture changed from yellow to black. After 24 h stirring, the dispersion was cooled down to room temperature. The received particles were collected by centrifugation (9000 rpm, 10 min) and resuspended in 1-propanol by using ultrasonication. The black particles were obtained after repeating this washing procedure six times. (Residual PVPVA content in the particles determined by C/N ratio in elemental analysis: P2 ≈ 8 wt%; P3 ≈ 7 wt%; P4 ≈ 0 wt%; P5 ≈ 1 wt%.)

Synthetic Procedure for 1,3-Bis(anilino)croconate[28]: In a 25 mL round-bottom flask, croconic acid (142.1 mg, 1 mmol) was dissolved in methanol (10 mL). The pale-yellow solution was heated to 60 °C and aniline (**6**) (186.3 mg, 2 mmol) was added to the hot solution. The reaction mixture was refluxed for 45 min with a color change from yellow to orange to red. The resulting red precipitation was filtered and washed with methanol (10 mL) and hot methanol (10 mL) three times. The product was obtained as red solid.

^{1}H NMR (400 MHz, DMSO-d_6, δ): 11.59 (s, 2H, R_2NH), 7.26–7.45 (m, 10 H, Ar H); MS (CI) m/z: 293.1 $(M+H)^+$.

NMR Spectroscopy: The ^{1}H NMR spectra were recorded on a 400 MHz Bruker Avance DRX 400 spectrometer using tetramethyl silane as internal standard. The chemical shifts (δ) in the ^{1}H NMR spectra were reported in parts per million (ppm) versus the residual proton content of the deuterated solvent at ambient temperature. The spin multiplicities were designated as follows: s = singlet, d = doublet, t = triplet, and m = multiplet. The obtained data were evaluated with the MestReNova program from Mestrelab Research.

UV/Vis Spectroscopy: UV/vis measurements were performed using a Lambda 365 spectrophotometer by Perkin Elmer with UV WinLab as standard software. The measurements were carried out within the wavelength range of 300–1100 nm with a scan speed of 600 nm min^{-1}. The samples were diluted in 1-propanol as standard solvent and measured in 1 cm quartz glass cuvettes.

Field Emission SEM: To determine the shape and size of the polymer particles, field emission SEM was performed with a Hitachi S-5200 Cryo-SEM. The samples were prepared by depositing the particle dispersions on a silicon wafer. After drying, the colloidal assemblies were sputtered with a 5–10 nm layer of platinum and measured with a constant acceleration voltage of 5 kV.

Mass Spectrometry: CI MS was performed on a Thermo Scientific ISQ LT using methane as reagent gas. MALDI-FTICR spectra were recorded on a solariX mass spectrometer (Bruker Daltonics) by using dithranol (50 mg mL^{-1} THF) as matrix.

PAI: Photoacoustic measurements were performed using the LED array light source PAI System by Cyberdyne LED with AcousticX as standard software. As light sources, high-density high-power LEDs with different wavelengths (750/850 nm and 820/940 nm) and selectable pulse widths of 30 up to 150 ns were utilized. The measurements were carried out with the speed of sound (1480 m s^{-1}) specific for water as the surrounding medium.

Cell Viability Studies: In order to determine cell viability, 20 000 HeLa cells, seeded into a μ-Slide 8 well plate (ibidi GmbH, Gräfelfing, Germany) were incubated for 4, 8, and 24 h with 300 μL phenol red-free DMEM, containing particles in a concentration of either 5, 100, or 200 μg mL^{-1}. Control cells were treated only with phenol red-free DMEM without particles. The supernatants were removed and the cells were washed with PBS. Subsequently, the cells were incubated in the dark for 5 min with 300 μL DMEM without phenol red and FCS containing fluorescein diacetate (8 μg mL^{-1}) and propidium iodide (20 μg mL^{-1}). The solution

was removed and cells were washed two times with PBS. From each well, images with a 10× magnification from three different positions were taken by using a Leica DMi8 confocal microscope. The cell images were analyzed using ImageJ. The cell viability was determined by dividing the amount of living cells by the total amount of cells.

Supporting Information

Supporting Information is available from the Wiley Online Library or from the author.

Acknowledgements

This work was supported by the Deutsche Forschungsgemeinschaft (DFG) in the framework of the Research Training Group "Tumor-Targeted Drug Delivery" grant 331065168. The authors thank Yonca Kayku for performing elemental analysis of the particles.

Open access funding enabled and organized by Projekt DEAL.

Conflict of Interest

The authors declare no conflict of interest.

Keywords

contrast agents, croconaine dyes, near-infrared absorbers, photoacoustic imaging, polymer nanoparticles

Received: August 3, 2020
Revised: September 28, 2020
Published online: October 12, 2020

[1] J. Liu, S. Wang, X. Cai, S. Zhou, B. Liu, *Chem. Commun.* **2018**, *54*, 2518.
[2] A. De La Zerda, C. Zavaleta, S. Keren, S. Vaithilingam, S. Bodapati, Z. Liu, J. Levi, B. R. Smith, T. J. Ma, O. Oralkan, Z. Cheng, X. Chen, H. Dai, B. T. Khuri-Yakub, S. S. Gambhir, *Nat. Nanotechnol.* **2008**, *3*, 557.
[3] E. Y. Zhou, H. J. Knox, C. Liu, W. Zhao, J. Chan, *J. Am. Chem. Soc.* **2019**, *141*, 17601.
[4] S. Mallidi, G. P. Luke, S. Emelianov, *Trends Biotechnol.* **2011**, *29*, 213.
[5] Y. Wang, N. Gong, Y. Li, Q. Lu, X. Wang, J. Li, *J. Am. Chem. Soc.* **2020**, *142*, 1735.
[6] L. V. Wang, S. Hu, *Science* **2012**, *335*, 1458.
[7] Y. S. Chen, S. J. Yoon, W. Frey, M. Dockery, S. Emelianov, *Nat. Commun.* **2017**, *8*, 15782.
[8] T. Stahl, R. Bofinger, I. Lam, K. J. Fallon, P. Johnson, O. Ogunlade, V. Vassileva, R. B. Pedley, P. C. Beard, H. C. Hailes, H. Bronstein, A. B. Tabor, *Bioconjugate Chem.* **2017**, *28*, 1734.
[9] G. Balasundaram, C. J. H. Ho, K. Li, W. Driessen, U. S. Dinish, C. L. Wong, V. Ntziachristos, B. Liu, M. Olivo, *Int. J. Nanomed.* **2015**, *10*, 387.
[10] P. Huang, J. Lin, W. Li, P. Rong, Z. Wang, S. Wang, X. Wang, X. Sun, M. Aronova, G. Niu, R. D. Leapman, Z. Nie, X. Chen, *Angew. Chem., Int. Ed.* **2013**, *52*, 13958.
[11] P. Beard, *Interface Focus* **2011**, *1*, 602.
[12] L. V. Wang, *Med. Phys.* **2008**, *35*, 5758.
[13] A. Danielli, K. Maslov, C. P. Favazza, J. Xia, L. V. Wang, *Appl. Phys. Lett.* **2015**, *106*, 203701.
[14] T. Repenko, A. Rix, A. Nedilko, J. Rose, A. Hermann, R. Vinokur, S. Moli, R. Cao-Milàn, M. Mayer, G. von Plessen, A. Fery, L. De Laporte, W. Lederle, D. N. Chigrin, A. J. C. Kuehne, *Adv. Funct. Mater.* **2018**, *28*, 1705607.
[15] K. Pu, A. J. Shuhendler, J. V. Jokerst, J. Mei, S. S. Gambhir, Z. Bao, J. Rao, *Nat. Nanotechnol.* **2014**, *9*, 233.
[16] X. Yang, C. Li, B. Yang, W. Wang, Y. Qian, *Chem. Phys. Lett.* **2004**, *383*, 502.
[17] X. Liang, Z. Deng, L. Jing, X. Li, Z. Dai, C. Li, M. Huang, *Chem. Commun.* **2013**, *49*, 11029.
[18] A. Liopo, R. Su, A. A. Oraevsky, *Photoacoustics* **2015**, *3*, 35.
[19] T. Repenko, S. Fokong, L. De Laporte, D. Go, F. Kiessling, T. Lammers, A. J. C. Kuehne, *Chem. Commun.* **2015**, *51*, 6084.
[20] Q. Zhang, N. Iwakuma, P. Sharma, B. M. Moudgil, C. Wu, J. McNeill, H. Jiang, S. R. Grobmyer, *Nanotechnology* **2009**, *20*, 395102.
[21] H. Yuan, C. G. Khoury, H. Hwang, C. M. Wilson, G. A. Grant, T. Vo-Dinh, *Nanotechnology* **2012**, *23*, 075102.
[22] F. Gao, L. Bai, X. Feng, H. P. Tham, R. Zhang, Y. Zhang, S. Liu, L. Zhao, Y. Zheng, Y. Zhao, *Small* **2016**, *12*, 5239.
[23] Y. Yan, J. Chen, Z. Yang, X. Zhang, Z. Liu, J. Hua, *J. Mater. Chem. B* **2018**, *6*, 7420.
[24] D. E. Lynch, D. G. Hamilton, *Eur. J. Org. Chem.* **2017**, *2017*, 3897.
[25] E. E. Havinga, W. ten Hoeve, H. Wynberg, *Polym. Bull.* **1992**, *29*, 119.
[26] E. E. Havinga, W. ten Hoeve, H. Wijnberg, *US 5380807*, **1995**.
[27] L. Tang, X. Sun, N. Liu, Z. Zhou, F. Yu, X. Zhang, X. Sun, X. Chen, *ACS Appl. Nano Mater.* **2018**, *1*, 1741.
[28] C. Prabhakar, Promila, A. Tripathi, K. Bhanuprakash, V. Jayathirtharao, *J. Mol. Struct.* **2017**, *1146*, 684.
[29] A. J. C. Kuehne, M. C. Gather, J. Sprakel, *Nat. Commun.* **2012**, *3*, 1087.
[30] R. R. Rosencrantz, K. Rahimi, A. J. C. Kuehne, *J. Phys. Chem. B* **2014**, *118*, 6324.
[31] F. Würthner, T. E. Kaiser, C. R. Saha-Möller, *Angew. Chem., Int. Ed.* **2011**, *50*, 3376.
[32] S. Ciftci, A. J. C. Kuehne, *Macromolecules* **2015**, *48*, 8389.
[33] H. Kobayashi, M. Ogawa, R. Alford, P. L. Choyke, Y. Urano, *Chem. Rev.* **2010**, *110*, 2620.
[34] Y. Dong, Y. Tu, K. Wang, C. Xu, Y. Yuan, J. Wang, *Angew. Chem., Int. Ed.* **2020**, *59*, 7168.
[35] K. Klyukin, V. Alexandrov, *Proteins* **2020**, *88*, 1162.